

The MaGICC volume: reproducing statistical properties of high redshift galaxies

Rahul Kannan^{1*}†, Greg S. Stinson¹, Andrea V. Macciò¹, Chris Brook²,
Simone M. Weinmann³, James Wadsley⁴, Hugh M. P. Couchman⁴

¹ *Max-Planck-Institut für Astronomie, Königstuhl 17, 69117 Heidelberg, Germany*

² *Departamento de Física Teórica, Universidad Autónoma de Madrid, E-28049 Cantoblanco, Madrid, Spain*

³ *Leiden Observatory, Leiden University, P.O. Box 9513, 2300 RA Leiden, The Netherlands*

⁴ *Department of Physics and Astronomy, McMaster University, Hamilton, Ontario, L8S 4M1, Canada*

13 February 2013

ABSTRACT

We present a cosmological hydrodynamical simulation of a representative volume of the Universe, as part of the Making Galaxies in a Cosmological Context (MaGICC) project. MaGICC uses a sub-grid feedback model that includes a thermal implementation of both supernova + early (pre-supernova) stellar feedback that matches the observed stellar mass evolution of an L_* galaxy at high resolution. The large volume simulation tests the stellar feedback at lower resolution across a wide range of galaxy masses, morphologies, environments and merging histories.

The simulated sample compares well with a wide range of observed relations of high redshift galaxies ($z \geq 2$). It matches the slope and scatter in the stellar mass–halo mass ($M_* - M_h$) relation and the Galaxy Stellar Mass Function (GSMF) for low mass ($M_* < 5 \times 10^{10} M_\odot$) galaxies. The observed number density evolution of low mass galaxies is reproduced in our simulation, suggesting that our feedback implementation naturally detaches stellar mass growth from dark matter accretion history, which is a major improvement in galaxy formation models. The poor match of the $M_* - M_h$ and the GSMF at high masses ($M_* \geq 5 \times 10^{10} M_\odot$) indicates that thermal feedback is not sufficient to limit star formation in these haloes. The simulations match the observed star formation history of the Universe and the star forming main sequence ($SFR - M^*$). We see an increased specific star formation rate (sSFR) with redshift, in good agreement with observations that are corrected for nebular emission lines, although the simulations fall below the relation at $z = 2$. Altogether our results suggest that early stellar feedback, in conjunction with supernovae feedback, plays a major role in regulating the properties of low mass galaxies at high redshift.

Key words: galaxies: formation – galaxies: evolution, interactions, structure – methods: numerical – methods: N-body simulations

1 INTRODUCTION

Gravitational assembly of structure in a Lambda Cold Dark Matter (ΛCDM) Universe is well understood and mostly consistent with observations. However, the evolution of galaxies inside dark matter haloes presents many challenges for modellers. The baryonic physics in haloes is complicated,

involving various processes such as gas cooling, star formation, radiative transfer, stellar and active galactic nucleus (AGN) feedback. These processes are highly non-linear and modelling them accurately is the major challenge for galaxy formation theory.

Fortunately, there are now large catalogues of galactic data available at every epoch of cosmic history. They make it possible to compare galaxy formation models with observations, throughout their evolution. These catalogues include observations that present full spectral energy distributions of the galaxies from 1.4 GHz radio continuum observations with the *VLA* (Karim et al. 2011), to infrared imaging with *Hubble/WFC3*, *Spitzer/MIPS* and *VLT/HAWK-I*

* Member of the International Max Planck Research School for Astronomy and Cosmic Physics at the University of Heidelberg (IMPRS-HD) and the Heidelberg Graduate School of Fundamental Physics (HGSFP)

† kannan@mpia.de

(Kajisawa et al. 2010; Santini et al. 2012). These observations give a complete picture of star formation even when it is dust obscured.

From these observations, one can construct a cosmic star formation history to compare with models (Lilly et al. 1996; Madau et al. 1996; Hopkins 2004; Wilkins et al. 2008; Bouwens et al. 2012). The shape of the cosmic star formation history has a steep rise from $z = 0$ to $z = 1$ before flattening off and then steadily decreasing from $z = 2$ to higher redshift.

It is also possible to compare the star formation rate (SFR) of individual galaxies with their stellar mass (M_*) determined from infrared photometry. In observations, SFR and M_* show a tight correlation that is sometimes called the star forming main sequence (Brinchmann et al. 2004; Noeske et al. 2007; Wuyts et al. 2011). The slope of the relationship does not evolve significantly with redshift, but the normalization increases at higher redshifts (Whitaker et al. 2011; Kajisawa et al. 2010).

Dividing the SFR by M_* gives the specific star formation rate (sSFR), which provides a test of the star formation efficiency compared to prior star formation. Similar to the rise of the star forming main sequence, the sSFR rises with redshift (Karim et al. 2011; Kajisawa et al. 2010). Above $z = 2$, some observations show that the evolution of the sSFR flattens, though Stark et al. (2013) found that when corrected for nebular line emission, the sSFR continues increasing up to $z = 7$.

The primary constraint used for many models is the number density of galaxies as a function of their stellar mass, the galaxy stellar mass function (hereafter, GSMF). The GSMF is a Schechter type function characterized by a power law at low masses and an exponential cutoff. At $z = 0$, the exponential cutoff is at $M_* \sim 5 \times 10^{10} M_\odot$ (Li & White 2009). The GSMF evolves as a function of redshift: Santini et al. (2012) find that the low mass slope increases with redshift while Peng et al. (2010) finds that the slope remains constant, but the normalization increases.

Three types of models are commonly used to understand how stars populate galaxies:

- Statistical models: compare statistics of simulations with observations
- Semi-analytic models: populate dark matter haloes with stars based on halo mass, merger history, and single zone physics
- Cosmological simulations: Model a volume of the Universe with hydrodynamics

1.1 Statistical Models

The statistical models are based on comparing the GSMF with the dark matter halo mass function and lead to an understanding of how efficiently stars form as a function of dark matter halo mass. A set of cosmological parameters makes explicit predictions about the mass function (Press & Schechter 1974; Sheth et al. 2001; Reed et al. 2005) of dark matter haloes and how those haloes are distributed throughout the Universe. The observed GSMF has a different shape than the dark matter halo mass function found in simulations. The GSMF low mass slope (α) is shallower than the low mass dark matter mass function slope. The

$M_* \sim 5 \times 10^{10} M_\odot$ cutoff is at a lower mass than the dark matter mass function exponential cutoff.

Halo Occupation Models make the reasonable assumption that the distribution of galaxies in the Universe is similar to the distribution of dark matter haloes, modulo some bias (Peacock & Smith 2000). Halo Occupation Models attempt to match the correlation function statistics of galaxies and dark matter haloes to determine the stellar mass of galaxies that are most likely to be present in a particular dark matter halo. Using Halo Occupation Modelling, one can construct a Conditional Luminosity Function that can be compared with the real luminosity function (Yang et al. 2003; van den Bosch et al. 2007).

Conroy et al. (2006) realized that if one used satellite masses at their time of accretion, then the clustering statistics of mass-ordered dark matter halo samples matches galaxies. This realization led to the abundance matching technique in which galaxies are placed in dark matter haloes with the same stellar mass ranking as that of the dark matter halo mass rank (Conroy & Wechsler 2009; Moster et al. 2010; Guo et al. 2010; Behroozi et al. 2010). Such a match leads to the *stellar mass-halo mass* ($M_* - M_h$) relationship, the key constraint for our model. The $M_* - M_h$ relation consists of two power laws with a steep slope at low masses and shallow slope at high masses. Stars form most efficiently at the break mass. The star formation efficiency drops quickly to both higher and lower masses. The characteristic mass of the break in the power law is $M_{halo} \sim 10^{12} M_\odot$ at $z = 0$ (Moster et al. 2013).

The availability of luminosity functions at high redshifts means that we can trace the evolution of the $M_* - M_h$ relation. Abundance matching indicates that the $M_* - M_h$ relation evolves surprisingly little (Behroozi et al. 2013). The star formation efficiency evolves most significantly to higher halo masses at higher redshift from $M_h \sim 10^{12} M_\odot$ at $z = 0$ to $M_h \sim 10^{12.5} M_\odot$ at $z = 3$ (Moster et al. 2013; Behroozi et al. 2012).

The key finding of the abundance matching models is that the star formation peaks earliest in the highest mass galaxies whereas, in the lowest mass galaxies, the SFR increases monotonically with time. This is a reflection of galaxy downsizing. This represents a delay of star formation in low mass halos and is the most important feature that must be reproduced in models in order to get the evolution of low mass galaxies right.

1.2 Semi-Analytic Models

Semi-Analytic Models (SAMs) try to match the GSMF at $z = 0$ using physical prescriptions based on the mass and merger history of dark matter haloes taken from simulations (Kauffmann et al. 1993). SAMs show that supernovae can limit star formation in low mass galaxies (White & Rees 1978; White & Frenk 1991; Somerville & Primack 1999; Benson et al. 2003) and that active galactic nuclei (AGN) can limit star formation in high mass galaxies (e.g. De Lucia et al. 2006; Bower et al. 2006).

While SAMs do well matching the evolution of the high mass luminosity function, they do not match the evolution of low mass galaxies at high redshift (Guo et al. 2011). Current SAMs include strong stellar feedback to reproduce the GSMF at $z = 0$ (e.g. Guo et al. 2011; Bower et al. 2012),

but the low and intermediate mass galaxies build their stellar mass at early times ($z > 2$) following the assembly of the dark matter mass, because the feedback mechanism in these SAMs do not delay star formation in low mass halos. That means that there is little evolution in the SAM luminosity functions after $z = 2$, in contrast with observations (e.g. Fontanot et al. 2009; Marchesini et al. 2009; Guo et al. 2011). The early star formation means the SAM galaxies have low specific star formation rates at $z < 2$ (e.g. Daddi et al. 2007; Damen et al. 2009) and high values at $z > 3$ (e.g. Bouché et al. 2010; Dutton et al. 2010; Weinmann et al. 2011) although this picture might change at high redshifts due to refinement in the observational estimates of sSFR (Stark et al. 2013). This discrepancy has been looked at in detail by Weinmann et al. (2012), who use the number density evolution of low mass ($9.27 < \log(M_*/M_\odot) < 9.77$) galaxies as a diagnostic to find that the observed evolution of the number density is not reproduced in any SAMs or simulations. They argue that the simple supernova feedback mechanism used in these models that gets the present day GSMF correct does not decouple star formation from the parent DM halo growth.

1.3 Simulations

Hydrodynamical simulations model galaxy formation with more resolution than SAMs and include self-consistent interaction of dark matter and baryon evolution. Although the efficiency of computational calculations has increased, it is still not possible to resolve many important physical processes, so they must be modelled at the ‘sub-grid’ level. These processes include gas cooling, star formation and stellar feedback.

Since relatively little is known about star formation and feedback, the models include free parameters, which are constrained by observations. Star formation model parameters are constrained using local observations of the Kennicutt-Schmidt gas density–star formation density relation (Springel & Hernquist 2003; Stinson et al. 2006; Schaye & Dalla Vecchia 2008). The energy feedback from stars is modelled either by adding velocity to gas, called *kinetic feedback*, or adding thermal energy and delaying cooling, called *thermal feedback*. These models have been constrained based on observations (Springel & Hernquist 2003; Oppenheimer & Davé 2006; Dalla Vecchia & Schaye 2008; Crain et al. 2009; McCarthy et al. 2012). The model used in this paper instead constrains stellar feedback to match the evolution of $M_* - M_h$ relation.

There has been a lot of research on the optimal velocity for winds driven using kinetic feedback. The original models used a fixed wind velocity (Springel & Hernquist 2003; Crain et al. 2009; McCarthy et al. 2012), however, they had difficulties reproducing the GSMF at $z = 0$. Observations of metal absorption lines in outflows show that wind velocities are not constant, but are correlated with star formation rate, $v_w \approx SFR^{0.35}$, at $z = 0$ (Martin 2005) and $v_w \approx SFR^{0.3}$ at $z \approx 1.4$ (Weiner et al. 2009). These observations motivated using momentum conserving wind models in which mass loading depends on the mass of the host galaxy such that $\dot{M}_{wind}/\dot{M}_* \propto V_{circ}^{-1}$ (Oppenheimer & Davé 2006; Oppenheimer & Davé 2008; Davé et al. 2011a,b). Momentum conserving winds successfully reproduce the GSMF

and many other observed galaxy properties at $z = 0$ (Oppenheimer et al. 2010; Davé et al. 2011a,b; Puchwein & Springel 2013), but has similar shortcomings with the low mass end of the luminosity function as the SAMs at high redshift. Weinmann et al. (2012) conclude that the current models of stellar feedback (in both SAMs and simulations) are unlikely to decouple the galaxy and DM halo growth due to its fundamental dependence on host halo mass and accretion history.

In thermal feedback, stars heat the surrounding gas particles adiabatically, which builds up pressure that can push gas out of galaxies (Gerritsen & Icke 1997; Thacker & Couchman 2000; Kawata & Gibson 2003; Stinson et al. 2006). Since stars form in very dense regions, the cooling time of the surrounding gas is short, making it necessary to account for unresolved inhomogeneities in the inter stellar medium. One method to account for such ‘sub-grid’ physics is to delay cooling within the blast radius of supernovae. Simulations using thermal feedback have so far focused on disk structure using high resolution zoom in simulations (Governato et al. 2010; Brook et al. 2011; Sawala et al. 2011; Guedes et al. 2011; Agertz et al. 2011). Some recent simulations of a handful of galaxies have indicated that adiabatic feedback produces galaxies that follow $M_* - M_h$ below $M_{halo} < 10^{12}M_\odot$ (Brook et al. 2012; Munshi et al. 2012).

In most models of stellar feedback, only feedback from supernovae is considered, but Murray et al. (2010) recognized the amount stars can disrupt molecular clouds before any stars explode as supernovae. Hopkins et al. (2011) and Agertz et al. (2012) implemented early stellar feedback schemes that rely on IR radiation pressure and tested them on isolated galaxy simulations. Lopez et al. (2011) and Pellegrini et al. (2011) found that when they mapped the pressure in different phases of the gas in the 30 Doradus region of the LMC, UV photoheating provides more pressure than IR radiation pressure.

In Stinson et al. (2013), we assume that photo-heating from massive stars is thermalised by the time it reaches the spatial scales resolved in cosmological simulations. So, we inject thermal energy equal to the fraction of the bolometric luminosity emitted in the UV in the time between the formation of the star and the first supernova explosion. This early stellar feedback limits star formation to the amount prescribed by the $M_* - M_h$ relationship and delays star formation in an L_* galaxy, so that the galaxy follows the evolution of the $M_* - M_h$ relationship. This is a major improvement over previous galaxy formation models, as the delayed star formation means that star formation is decoupled from DM halo mass growth. Some side-effects of using early stellar feedback include transforming DM cusps to cores in galaxies up to L_* masses (Macciò et al. 2012) and populating the circum-galactic medium with hot metal enriched gas, matching OVI observations (Stinson et al. 2013).

In this paper, we explore how the early stellar feedback model, described in Stinson et al. (2013), affects the global properties of galaxies on a large scale. To study this we simulate a large volume of the Universe, 114 Mpc on a side, as part of the Making Galaxies in a Cosmological Context (MaGICC) project. This simulation tests the effectiveness of our model at low resolution across a wide range of galaxy masses, environments and merger histories. We compare the properties of the galaxies in our simulations with observed

statistical properties of high redshift galaxies like the GSMF, stellar to halo mass relationship, star formation rate, and the number density evolution of low mass galaxies through cosmic time. In Section 2 we briefly outline the star formation and stellar feedback mechanisms used in our simulations, in Section 3 we present our results at $z \geq 2$ and compare them to the current observational estimates. In Section 4 we summarize our results and discuss future challenges.

2 SIMULATION METHOD

We simulate a cosmological volume, 114 Mpc on a side, from $z = 99$ to $z = 2$. It is created using WMAP7 initial conditions with $(h, \Omega_M, \Omega_\Lambda, \Omega_b, \sigma_8) = (0.702, 0.2748, 0.7252, 0.0458, 0.816)$ (Larson et al. 2011; Komatsu et al. 2011). The simulation includes 512^3 dark matter and 512^3 gas particles. The dark matter particles each have masses of $3.4 \times 10^8 M_\odot$ and a softening length of ~ 3.7 kpc. Initially, gas particles each have masses of $6.9 \times 10^7 M_\odot$ and star particles initially have masses of $1.3 \times 10^7 M_\odot$. Gas and star particles have a softening length of ~ 2.17 kpc.

All the simulations use the smoothed particle hydrodynamics (SPH) code GASOLINE (Wadsley et al. 2004). Details of the physics used in the MaGICC project are detailed in Stinson et al. (2013). Briefly, stars are formed from gas cooler than $T_{max} = 10^4$ K, and denser than 9.6 cm^{-3} according to the Kennicutt Schmidt Law as described in Stinson et al. (2006) with $c_* = 0.1$.

The star particles are massive enough to represent an entire stellar population consisting of stars with masses given by the Chabrier (2003) initial mass function. 20% of these have masses greater than $8 M_\odot$ and explode as Type II supernovae from 4 until 35 Myr after the stellar population forms according to the Padova stellar lifetimes (Alongi et al. 1993; Bressan et al. 1993). Each supernova ejects $E_{SN} = 10^{51}$ ergs of purely thermal energy into the surrounding gas (~ 1 kpc at the resolution of our simulations). The supernova energy would be radiated away before it had any dynamical impact because of the high density of the star forming gas. Thus, the supernova feedback relies on delaying the cooling based on the sub-grid approximation of a blast wave as described in Stinson et al. (2006).

The supernovae feedback does not start until 3.5 Myr after the first massive star forms. However, nearby molecular clouds show evidence of being blown apart *before* any SNII exploded (Murray et al. 2011) and Lopez et al. (2011) and Pellegrini et al. (2011) found that most of the pressure comes from UV photoheating is the dominant feedback mechanism in early phases of star formation by mapping out the pressure in different phases of the gas. In simulations in the MaGICC project, like those here, 10% the UV luminosity of the stars is injected into the surrounding gas over this 3.5 Myr period without disabling the cooling. (Stinson et al. 2013) showed that this energy limits star formation to the amount prescribed by the $M_* - M_h$ relationship at all redshifts. The current work is our attempt explore how this star formation and feedback prescription works at lower resolutions over a wide range of galaxy masses.

2.1 Halo identification

For each snapshot, we find all the virialized haloes within the high resolution region using a Spherical Overdensity (SO) algorithm. Candidate groups with a minimum of $N_f = 100$ particles are selected using a FoF algorithm with linking length $\phi = 0.2d \approx 22$ kpc (d is the average particle separation). We then: (i) find the point C where the gravitational potential is a minimum; (ii) determine the radius \bar{r} of a sphere centered on C , where the density contrast is Δ_{vir} , with respect to the critical density of the Universe. Using all particles in the corresponding sphere, we iterate the above procedure until we converge onto a stable particle set. We use a time varying virial density contrast Δ_{vir} , whose value is determined using the fitting formula presented in Mainini et al. (2003), based on linear theory and the spherical top-hat collapse model. We include in the halo catalogue all the haloes with more than 100 particles (see Macciò et al. 2007, 2008 for further details on our halo finding procedure).

3 RESULTS

We compare the simulated galaxy population in a 114^3 Mpc³ volume with a set of basic properties derived from the most recent observational estimates. These include the galaxy stellar mass function (GSMF), stellar mass–halo mass ($M_* - M_h$) relationship, cosmic star formation history (SFH), star forming main sequence, and specific star formation rates (sSFRs). Individual galaxies have been shown to match observations well (Brook et al. 2012; Stinson et al. 2013), so the volume provides an opportunity to test the accuracy and effectiveness of this feedback model at low resolution and high redshift. All the observational estimates of stellar masses and SFRs, that our results have been matched to, have been corrected to a Chabrier (2003) IMF.

3.1 Stellar - halo mass ($M_* - M_h$) relation

Figure 1 shows the $M_* - M_h$ relation for all the galaxies in the simulated volume (black points) that contain a minimum of 20 star particles, or a stellar mass of $\sim 3 \times 10^8 M_\odot$. The galaxies trace the slope of the $M_* - M_h$ (green line) up to $M_{halo} = 10^{12} M_\odot$ at all redshifts where it has been examined. The scatter of the simulated galaxies also matches the variation in the relation as obtained by Moster et al. (2013) (grey shaded area). The agreement points to the fact that the stellar feedback effectively regulates star formation to produce the right amount of stellar mass in a given halo mass at all times.

Above a halo mass of $10^{12} M_\odot$, abundance matching (green line) shows a decrease in star formation efficiency. This is not reproduced in the simulation. The star formation efficiency actually increases at $M_{halo} \sim 4 \times 10^{12} M_\odot$, before decreasing slightly as represented by the slightly shallower slope of the simulation points. The reduced SFE is due to the reduced gas accretion because of the high virial gas temperature of the halo. However, this slight decrease in SFE does not reduce the star formation in these high mass haloes to the extent observed. The implemented stellar feedback model is insufficient in these high mass haloes.

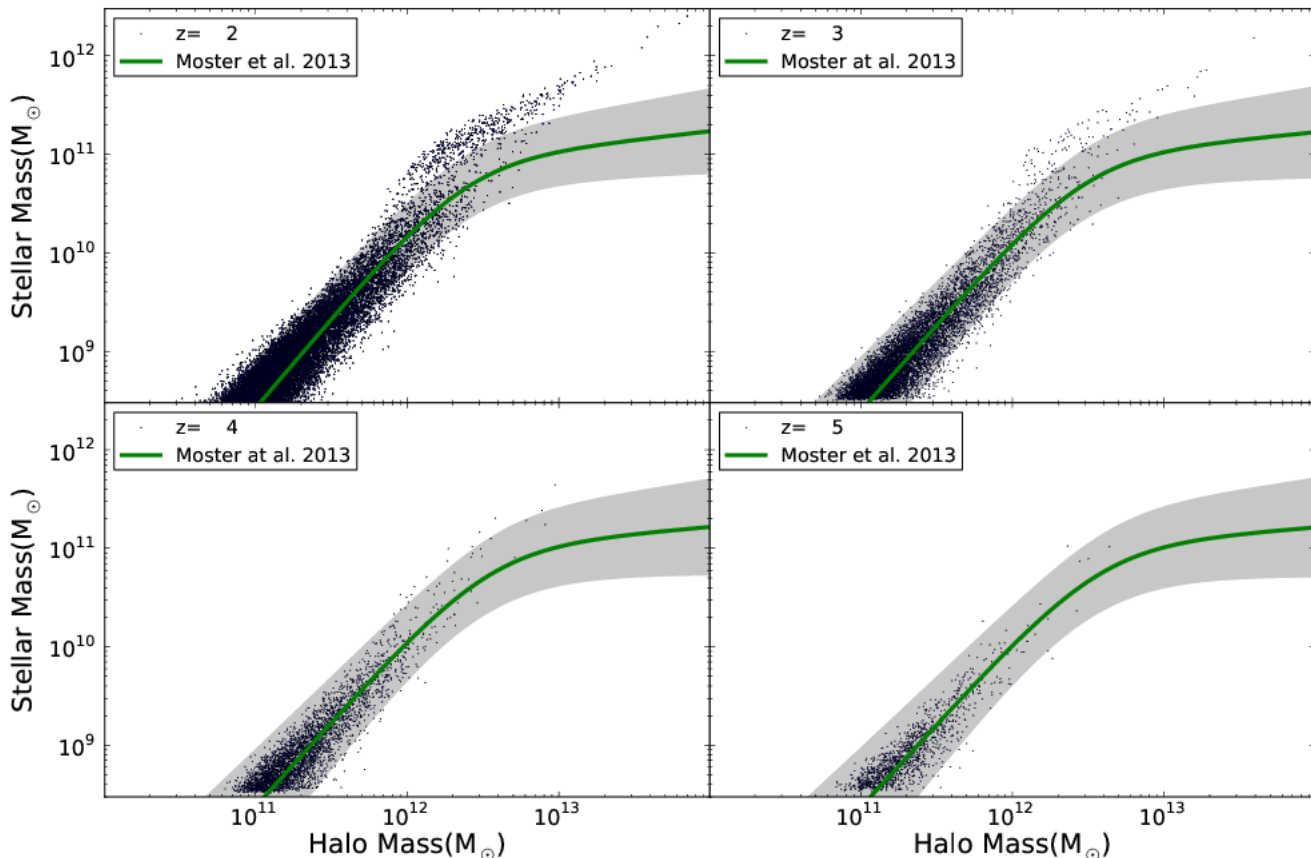


Figure 1. M_* – M_h relation at different redshifts. The blue points are simulated galaxies, the green line is the Moster et al. (2013) relation derived from abundance matching techniques and the grey shaded area is the scatter derived for the relation. Our simulated galaxies match the relation below $M_{halo} < 10^{12}M_{\odot}$, but star formation is too efficient in high mass haloes.

Some other quenching mechanism is required such as feedback from a central super-massive black hole (AGN feedback, e.g. Fanidakis et al. 2011; Springel et al. 2005).

3.2 The galaxy stellar mass function (GSMF)

The GSMF measures the number of galaxies of a certain stellar mass in a given volume of the Universe. The era of deep, high redshift surveys has provided detailed GSMFs out to $z = 3$. We compare our simulation results to Santini et al. (2012), who use deep *WFC3* near-IR data and deep *Hawk-I* K_S band data, to determine the low-mass end of the GSMF. The observed GSMFs are presented for various redshift ranges. To compare with them, we use the simulated GSMF from the middle of the observed redshift range. Figure 3 shows that the simulated galaxies (blue line) trace the low mass end of the observed GSMF (red points) very well. The feedback model makes the slope of the GSMF as shallow as the observed value, which is non-trivial and is a major improvement over previous attempts to match the GSMF at high redshift (e.g. Guo et al. 2011). A small discrepancy remains, as the simulated number density of high mass galaxies continues to decrease at the same rate,

whereas the observations show an exponential cutoff. This again indicates that stellar feedback is insufficient to limit star formation in these high mass haloes.

3.3 Number density evolution of low mass galaxies

Weinmann et al. (2012) used the number density evolution of low mass ($9.27 < \log(M_*/M_{\odot}) < 9.77$) galaxies to show that semi-analytic models or cosmological hydrodynamic simulations do not correctly model low mass galaxies. They argue that the simple supernova feedback mechanism changes the stellar mass at $z = 0$, but renormalizes the star formation history and thus does not decouple star formation from DM accretion. Stinson et al. (2013) showed for a single high resolution L^* simulation that early stellar feedback can break the coupling of star formation to dark matter accretion. Figure 3 shows the number density evolution of low mass galaxies at high redshifts in our simulation volume compared to observations taken from Figure 1 of Weinmann et al. (2012), as well with the SAM described in Guo et al. (2011). The simulation matches the observational results much better and lies well below the values obtained by the SAM. We note that

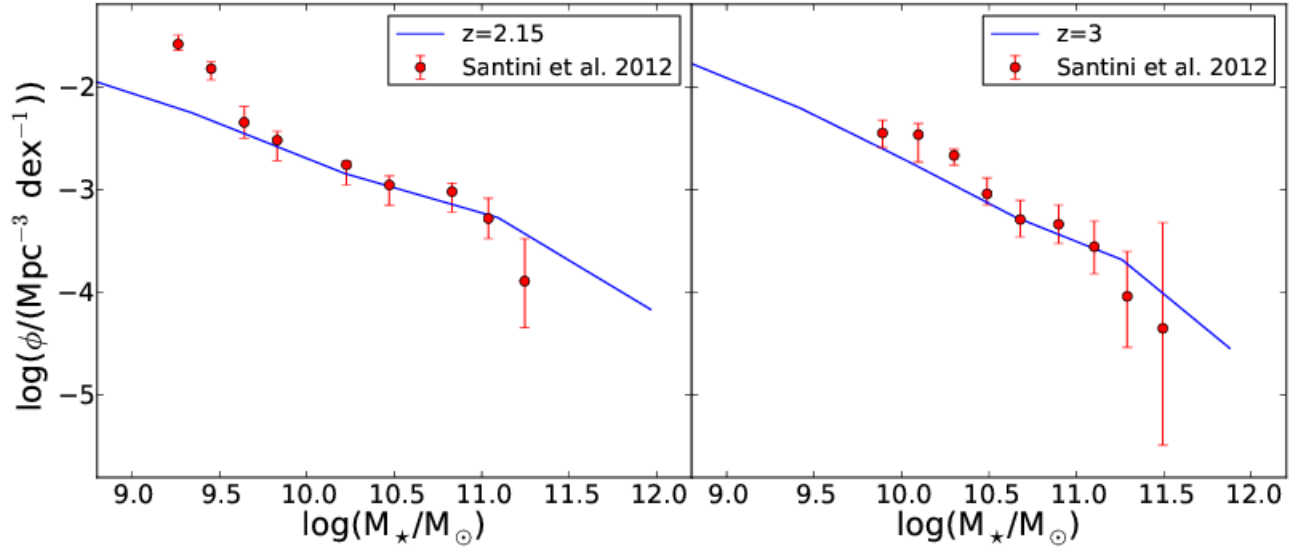


Figure 2. Galaxy stellar mass function at $z = 2$ & $z = 3$ (blue lines). The observational data points (red points) are taken from Santini et al. (2012). The low mass slope of the GSMF matches with observations, but there is no exponential decrease in the high mass end.

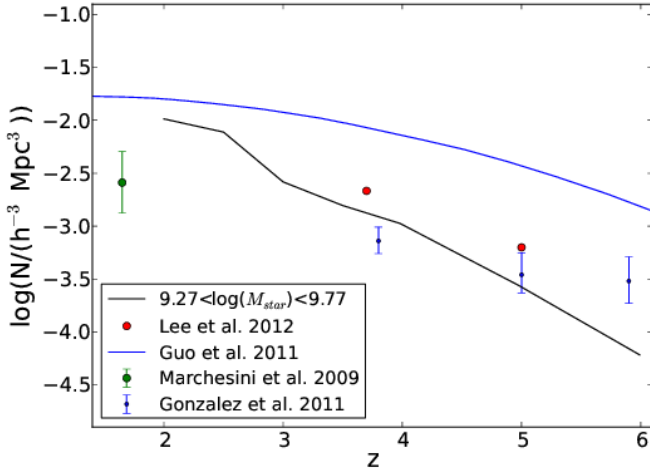


Figure 3. Number density of low mass galaxies as a function of redshift (black line) compared to various observational estimates (points) and a semi analytic model (green line) as described in Guo et al. (2011). Our simulation results go through the observational points, but the slope is steeper.

the slope obtained from our model is still slightly steeper than observed, indicating that the simulation is building low mass galaxies faster than observed.

3.4 Star formation History

We can also compare our simulation with the total number of stars formed in the Universe as a function of time. Figure 4 shows how the cosmic star formation rate evolves as a function of redshift ('Lilly-Madau plot') in our simulated volume. The observed points used for comparison are taken

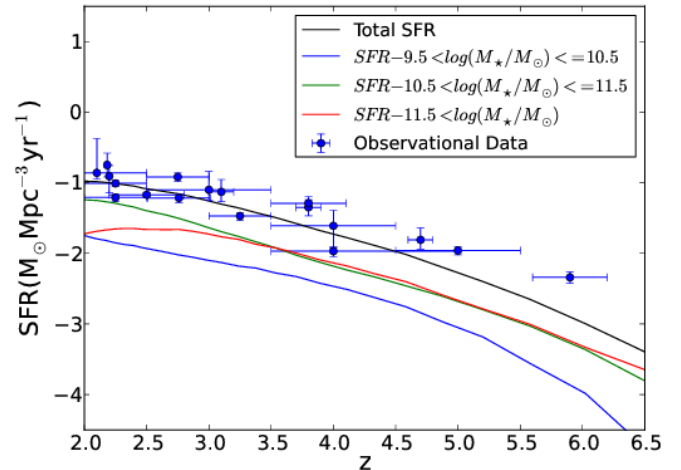


Figure 4. The evolution of the star formation rate density. The blue points are a compilation of star formation rate density estimates taken from Moster et al. (2013). The black solid line is our result for all galaxies, the blue line is the SFR density for low mass galaxies ($9.5 < \log(M_*/M_\odot) < 10.5$), the green for intermediate ($10.5 < \log(M_*/M_\odot) < 11.5$) mass galaxies and the red line for high mass ($\log(M_*/M_\odot) > 11.5$) galaxies. There is a clear trend of decreasing star formation at $z \lesssim 3.5$ in the highest mass galaxies.

from Moster et al. (2013) and include star formation estimates derived from rest frame UV (Salim et al. 2007; van der Burg et al. 2010; Robotham & Driver 2011; Bouwens et al. 2011; Cucciati et al. 2012), H α (Ly et al. 2011), combined UV and IR (Zheng et al. 2007; Kajisawa et al. 2010), FIR (Rujopakarn et al. 2010) and radio observations (Šmolčić et al. 2009; Dunne et al. 2009; Karim et al. 2011). The to-

tal SFR density (black line) passes through the observations from $z = 2 - 5$.

The total SFH can be divided into separate lines based on the stellar mass of the halo at $z = 2$ in which the stars are formed. The lowest mass galaxies ($9.5 < \log(M_*/M_\odot) < 10.5$) contribute little to the overall SFR density, while the intermediate ($10.5 < \log(M_*/M_\odot) < 11.5$) and high mass ($\log(M_*/M_\odot) > 11.5$) contribute equally up to $z = 3$. Below this redshift, the SFR flattens out in the highest mass galaxies. This flattening is not sufficient to explain the quenching of high mass galaxies as shown by the failure of the simulated $M_* - M_h$ and GSMF relations at the high mass end. We note that our match of the star formation history is not greatly affected by the excess star formation in galaxies with ($\log(M_*/M_\odot) > 11.5$) because even though the galaxies in that mass range form too many stars at $z \leq 3.5$, they are not the dominant population of galaxies at those redshifts.

3.5 Star forming main sequence

Observations show that star-forming galaxies have a tight correlation between their SFR and M_* (e.g., Elbaz et al. 2007; Pannella et al. 2009; Wuyts et al. 2011; Whitaker et al. 2012). This correlation has been called the “star forming main sequence.”

We compare the SFRs of our simulated galaxies with observational estimates by Kajisawa et al. (2010) and Whitaker et al. (2012). Kajisawa et al. (2010) studied SFR as a function of M_* for galaxies at $0.5 < z < 3.5$ in the GOODS-North field, using the K-selected sample from *Subaru*-MOIRCS. They determined SFRs from rest-frame, dust-corrected UV luminosity and the *Spitzer*-MIPS 24 μm flux. The depth of their data allowed them to constrain the slope of the SFR- M_* relation down to $M_* = 10^{9.5} M_\odot$ at $z \sim 3$. The median SFR as a function of stellar mass (green curve) from their sample of galaxies is plotted in top panels Fig. 5 at $z = 2$ & 3. The slope of their relation is close to unity for low mass galaxies at these high redshifts. Our simulated galaxies match these observations well at $z = 3$, but have nearly two times less star formation at $z = 2$. This discrepancy at $z = 2$ presents a challenge for all hydrodynamic simulations and SAMs (Weinmann et al. 2011). Davé (2008) suggested that an evolving stellar IMF is required to reduce the discrepancy in this relation out to $z = 2$.

Whitaker et al. (2012) measure star formation rates using the NEWFIRM Medium-Band Survey from MIPS 24 μm fluxes. At $z > 2$ their detection limit is $\log(M_*/M_\odot) > 10.7$. For these galaxies, they find a shallower, sub-linear, slope for their star forming main sequence, $SFR \propto M^{0.44}$, with a constant scatter of 0.34 dex. Above their detection limit, our simulated galaxies (black points) match the observations (red line) well as seen in the top left panel of Fig. 5.

3.6 Specific star formation rate evolution

Another common way to compare star formation rates with galaxy stellar masses is the specific star formation rate (sSFR), which gives the amount of star formation in haloes for a unit stellar mass of material. As one would expect from the star forming main sequence, the bottom panels of Fig. 5 show that the simulated galaxies (black points) match

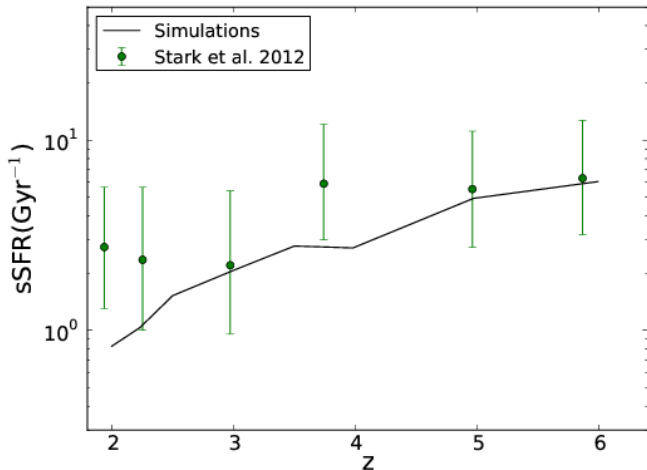


Figure 6. The evolution of the specific star formation rate for sample galaxies which have stellar masses within a narrow range around $\sim 5 \times 10^9 M_\odot$ (blackline). We compare the simulations with the observational estimates of Stark et al. (2013). The evolution of sSFR matches well at $z \leq 3$, but is below the observed value at lower redshifts.

the Kajisawa et al. (2010) (green curve) observed sSFRs at $z = 3$ but have ~ 2 times lower sSFR at $z = 2$. We also compare our simulated results with 1.4 GHz radio continuum observations from Karim et al. (2011) of star formation in galaxies in the 2 deg² COSMOS field. The simulated galaxies in our volume (black points) are in good agreement above $\log(M_*/M_\odot) > 10.7$, but are 2 – 3 times lower below this mass range at both $z = 2$ & 3.

Karim et al. (2011), like other authors before them (Stark et al. 2009; González et al. 2010), found that sSFR increases for galaxies in a given stellar mass range from $z = 0$ to $z \sim 2$, but then does not evolve much from $z = 2$ to $z \sim 7$. Weinmann et al. (2011) shows that such observations are contradictory with most models in which higher gas accretion rates at higher redshift and lower galaxy stellar masses translate into larger sSFR in galaxies within a fixed stellar mass range.

Stark et al. (2013) re-examined their data and found that their *Spitzer*-IRAC photometry was contaminated by nebular emission. They use the photometric excesses in the contaminated [3.6] filter to estimate the equivalent width distribution of H α emission at $3.8 < z < 5.0$. The corrected sSFRs increase from $z = 4$ to $z = 7$ by a factor of ~ 5 similar to what happens model predictions. Figure 6 shows the evolution of the sSFR in simulated galaxies (black line) within a narrow stellar mass range around $\sim 5 \times 10^9 M_\odot$. The simulation values are consistent with the corrected Stark et al. (2013) values (green points) for $z > 3$. However at $z < 3$ our simulation results are below the observed relation.

Many other authors find also find lower than observed sSFRs in their models (Davé 2008; Weinmann et al. 2012). The higher observed sSFRs again indicates delayed star formation in low mass galaxies. Although our model does a better job of delaying the star formation at early times than most SAMs and hydrodynamic simulations, below $z = 3$ the simulated haloes may still be forming too few stars.

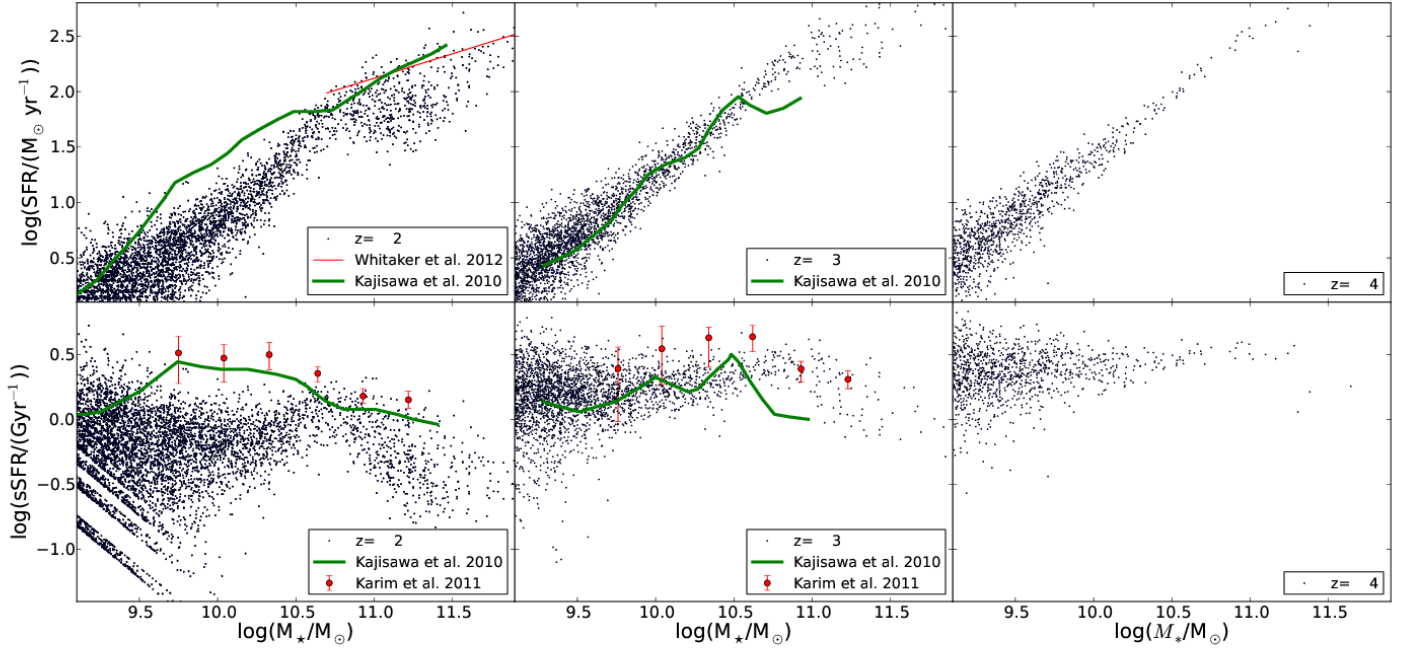


Figure 5. Top panels: The star forming main sequence (black points) at different redshifts. The $z = 2$ result for galaxies with $\log(M_*/M_\odot) > 10.7$ is matched to the observational results of Whitaker et al. (2012) (Red line). The slope of the main sequence is much steeper at lower masses. This matches well with the observational estimates derived by Kajisawa et al. (2010) at $z = 2&3$ (green curve). Bottom panels: The simulated sSFR (black points) matched to observational results matched from Karim et al. (2011) (Red points) and Kajisawa et al. (2010) (green curve). The simulated sSFR lies below the observed values for low mass galaxies at $z = 2$ by a factor of ~ 2 , but matches very well at $z = 3$.

This suggests the importance of some other physical mechanism, not modelled in our simulation, like the dependence of the star formation on gas metallicity (Krumholz et al. 2011; Krumholz & Dekel 2012), that could further delay star formation at earlier times and increase the sSFR of these galaxies at $z = 2$.

4 DISCUSSION AND CONCLUSIONS

We examine the effect of early stellar feedback used in the Making Galaxies in a Cosmological Context (MaGICC) project on a broad sample of galaxies in a cosmological volume of 114^3 Mpc^3 . The stellar feedback used is exactly the same as that used for a high resolution L_* galaxy. We compare the simulated galaxies with the observed $M_* - M_h$ relation, the galaxy stellar mass function, the cosmic star formation history, the star forming main sequence and the specific star formation rate. The simulated galaxies do a good job matching each observation to $z = 2$, the time when previous models have most deviated from observations. Our use of thermal stellar feedback is the key difference between our simulation and ones run previously. The way that it delays star formation in $M_h < 10^{12} M_\odot$ galaxies allows the simulations to match the observations.

Our simulation does not yet follow the evolution of the galaxy population all the way to $z = 0$, but we think the results at $z = 2$ are significant enough to report and it will take a significant amount of time for the simulation to reach

$z = 0$. We are encouraged by our previous simulations of the evolution of individual high resolution galaxies using the same stellar feedback match the evolution of an L_* galaxy (Brook et al. 2012; Stinson et al. 2013). It seems likely that our simulated low resolution galaxies will also continue to match the low mass end of the galaxy stellar mass function at $z = 0$. We plan to address this point in detail in a forthcoming paper.

The simulated galaxies not only follow the $M_* - M_h$ for $M_h < 10^{12} M_\odot$ at all the redshifts examined but also match the scatter in the relation. Correspondingly, the simulated galaxies match the shallow slope at the low mass end of the galaxy stellar mass function. The slope of the GSMF relationship was not a constraint for the simulation, but is a natural by product of the stellar feedback recipe used. It is a major improvement over previous attempts to match the GSMF at high redshift. The early stellar feedback decouples the growth of stellar mass from DM mass by effectively blowing the gas away from the disc either into the circum-galactic medium or entirely out of the halo. This helps regulate the number density of low mass galaxies to the observed values by delaying star formation in these haloes.

The simulated star formation history of the Universe also matches a variety of different observations. The model predicts that the lowest mass galaxies ($9.5 < \log(M_*/M_\odot) < 10.5$) contribute little to the overall SFR density, while the intermediate ($10.5 < \log(M_*/M_\odot) < 11.5$) and high mass ($\log(M_*/M_\odot) > 11.5$) galaxies contribute equally up to $z =$

3. After $z = 3$, the star formation slows in the highest mass galaxies.

At $M_h > 10^{12} M_\odot$, too many stars form, which is shown by the presence of galaxies above the abundance matching $M_* - M_h$ relation and the lack of an exponential cutoff in the GSMF. These indicate that the thermal stellar feedback is unable to quench star formation like is observed in massive galaxies.

Comparing SFR with stellar mass, the simulated galaxies lie along a tightly correlated “star forming main sequence.” The simulated galaxies match observations by Kajisawa et al. (2010) at $z \geq 3$, but there is a slight discrepancy at $z = 2$ between simulations and observations. At a given stellar mass, the simulated SFRs and correspondingly, the sSFRs, are ~ 2 times lower than the observed values at $9.5 < \log(M_*/M_\odot) < 10.5$. The high sSFRs in low mass haloes at $z = 2$ suggests that there needs to be a significant amount of cold gas still present in these galaxies at $z = 2$. Although our model does a better job of delaying the star formation at early times than most SAMs and hydrodynamic simulations, after $z = 3$ the simulated galaxies are forming too few stars.

Davé (2008) showed that the higher observed SFRs at $z \leq 2$ can be explained by an evolving stellar IMF, which becomes increasingly bottom-light at high redshift. However, Marchesini et al. (2009) showed that when such a bottom light IMF was used to model observations, the resulting observed high-redshift GSMF contained less galaxies, making the discrepancy with model GSMFs worse.

Regarding the evolution of sSFRs at $z > 3$, our simulation results are consistent with the revised Stark et al. (2013) observations for a sample of galaxies with stellar masses centred around $5 \times 10^9 M_\odot$. The increasing sSFR at $z \geq 4$ is consistent with increasing baryon accretion rates at larger redshift translating into larger sSFR in galaxies of fixed stellar mass. However, our simulated galaxies have lower sSFR values than observed at $z = 2$. Weinmann et al. (2012) argued that the correct sSFR evolution should follow naturally from the correct evolution of the GSMF. We see a slight deviation from the observed sSFR relation even though we match the GSMF. It must be noted that Weinmann et al. (2012) performed their analysis at $z < 2$, while our simulation has only reached at $z = 2$, where the observational estimates are less robust and might show some internal inconsistency among different galaxy properties (e.g. sSFR and GSMF).

There may also be another physical mechanism delaying star formation. Krumholz et al. (2011) and Krumholz & Dekel (2012) argue that star formation depends sensitively on a metallicity threshold. Until gas reaches this threshold, which coincidentally also delays the formation of H_2 , star formation is delayed in low mass galaxies at $z > 3$, which leaves sufficient cold gas at $z = 2$ to increase the sSFR of these galaxies to the observed values.

Altogether our results suggest that stellar feedback is one of the most important factors regulating star formation in $M_{halo} < 10^{12} M_\odot$ galaxies. What is most important is *when* the feedback occurs rather than simply the amount of feedback energy. Simply increasing and decreasing the feedback energy will only set the normalisation i.e., the total stellar mass of present at $z = 0$, but the key is delaying star formation in low mass galaxies. When we include stel-

lar feedback immediately after a star forms until supernovae stop exploding after 30 Myr, star formation is significantly delayed in low mass galaxies. In this way, we account for the downsizing in galaxy populations by delaying the star formation in low mass galaxies with our stellar feedback model and thus reconcile a couple key aspects of a Λ CDM cosmology with observations.

ACKNOWLEDGEMENTS

We are grateful to Ben Moster for providing his data in electronic format. We thank Arjen van der Wel and Aaron Dutton for valuable discussions. The simulations were performed on the THEO cluster of the Max-Planck-Institut für Astronomie at the Rechenzentrum in Garching; the clusters hosted on SHARCNET, part of ComputeCanada. We greatly appreciate the contributions of these computing allocations. RK, AVM and GS also acknowledge support from SFB 881 “The Milky Way System” (subproject A1) of the German Research Foundation (DFG). CBB acknowledges Max-Planck-Institut für Astronomie for its hospitality and financial support through the Sonderforschungsbereich SFB 881 (subproject A1) of the DFG.

REFERENCES

- Agertz O., Kravtsov A. V., Leitner S. N., Gnedin N. Y., 2012, ArXiv e-prints
- Agertz O., Teyssier R., Moore B., 2011, MNRAS, 410, 1391
- Alongi M., Bertelli G., Bressan A., Chiosi C., Fagotto F., Greggio L., Nasi E., 1993, A&AS, 97, 851
- Behroozi P. S., Conroy C., Wechsler R. H., 2010, ApJ, 717, 379
- Behroozi P. S., Wechsler R. H., Conroy C., 2012, ArXiv e-prints
- Behroozi P. S., Wechsler R. H., Conroy C., 2013, ApJL, 762, L31
- Benson A. J., Bower R. G., Frenk C. S., Lacey C. G., Baugh C. M., Cole S., 2003, ApJ, 599, 38
- Bouché N. et al., 2010, ApJ, 718, 1001
- Bouwens R. et al., 2012, ArXiv e-prints
- Bouwens R. J. et al., 2011, ApJ, 737, 90
- Bower R. G., Benson A. J., Crain R. A., 2012, MNRAS, 422, 2816
- Bower R. G., Benson A. J., Malbon R., Helly J. C., Frenk C. S., Baugh C. M., Cole S., Lacey C. G., 2006, MNRAS, 370, 645
- Bressan A., Fagotto F., Bertelli G., Chiosi C., 1993, A&AS, 100, 647
- Brinchmann J., Charlot S., White S. D. M., Tremonti C., Kauffmann G., Heckman T., Brinkmann J., 2004, MNRAS, 351, 1151
- Brook C. B. et al., 2011, MNRAS, 415, 1051
- Brook C. B., Stinson G., Gibson B. K., Wadsley J., Quinn T., 2012, MNRAS, 424, 1275
- Chabrier G., 2003, PASP, 115, 763
- Conroy C., Wechsler R. H., 2009, ApJ, 696, 620
- Conroy C., Wechsler R. H., Kravtsov A. V., 2006, ApJ, 647, 201
- Crain R. A. et al., 2009, MNRAS, 399, 1773

- Cucciati O. et al., 2012, *A&A*, 539, A31
Daddi E. et al., 2007, *ApJ*, 670, 156
Dalla Vecchia C., Schaye J., 2008, *MNRAS*, 387, 1431
Damen M., Förster Schreiber N. M., Franx M., Labbé I., Toft S., van Dokkum P. G., Wuyts S., 2009, *ApJ*, 705, 617
Davé R., 2008, *MNRAS*, 385, 147
Davé R., Finlator K., Oppenheimer B. D., 2011a, *MNRAS*, 416, 1354
Davé R., Oppenheimer B. D., Finlator K., 2011b, *MNRAS*, 415, 11
De Lucia G., Springel V., White S. D. M., Croton D., Kauffmann G., 2006, *MNRAS*, 366, 499
Dunne L. et al., 2009, *MNRAS*, 394, 3
Dutton A. A., van den Bosch F. C., Dekel A., 2010, *MNRAS*, 405, 1690
Elbaz D. et al., 2007, *A&A*, 468, 33
Fanidakis N., Baugh C. M., Benson A. J., Bower R. G., Cole S., Done C., Frenk C. S., 2011, *MNRAS*, 410, 53
Fontanot F., De Lucia G., Monaco P., Somerville R. S., Santini P., 2009, *MNRAS*, 397, 1776
Gerritsen J., Icke V., 1997, in *Revista Mexicana de Astronomia y Astrofisica Conference Series*, Vol. 6, *Revista Mexicana de Astronomia y Astrofisica Conference Series*, Franco J., Terlevich R., Serrano A., eds., p. 261
González V., Labbé I., Bouwens R. J., Illingworth G., Franx M., Kriek M., Brammer G. B., 2010, *ApJ*, 713, 115
Governato F. et al., 2010, *Nature*, 463, 203
Guedes J., Callegari S., Madau P., Mayer L., 2011, *ApJ*, 742, 76
Guo Q. et al., 2011, *MNRAS*, 413, 101
Guo Q., White S., Li C., Boylan-Kolchin M., 2010, *MNRAS*, 404, 1111
Hopkins A. M., 2004, *ApJ*, 615, 209
Hopkins P. F., Quataert E., Murray N., 2011, *MNRAS*, 417, 950
Kajisawa M., Ichikawa T., Yamada T., Uchimoto Y. K., Yoshikawa T., Akiyama M., Onodera M., 2010, *ApJ*, 723, 129
Karim A. et al., 2011, *ApJ*, 730, 61
Kauffmann G., White S. D. M., Guiderdoni B., 1993, *MNRAS*, 264, 201
Kawata D., Gibson B. K., 2003, *MNRAS*, 340, 908
Komatsu E. et al., 2011, *ApJS*, 192, 18
Krumholz M. R., Dekel A., 2012, *ApJ*, 753, 16
Krumholz M. R., Leroy A. K., McKee C. F., 2011, *ApJ*, 731, 25
Larson D. et al., 2011, *ApJS*, 192, 16
Li C., White S. D. M., 2009, *MNRAS*, 398, 2177
Lilly S. J., Le Fevre O., Hammer F., Crampton D., 1996, *ApJL*, 460, L1
Lopez L. A., Krumholz M. R., Bolatto A. D., Prochaska J. X., Ramirez-Ruiz E., 2011, *ApJ*, 731, 91
Ly C., Lee J. C., Dale D. A., Momcheva I., Salim S., Staudaher S., Moore C. A., Finn R., 2011, *ApJ*, 726, 109
Macciò A. V., Dutton A. A., van den Bosch F. C., 2008, *MNRAS*, 391, 1940
Macciò A. V., Dutton A. A., van den Bosch F. C., Moore B., Potter D., Stadel J., 2007, *MNRAS*, 378, 55
Macciò A. V., Stinson G., Brook C. B., Wadsley J., Couchman H. M. P., Shen S., Gibson B. K., Quinn T., 2012, *ApJL*, 744, L9
Madau P., Ferguson H. C., Dickinson M. E., Giavalisco M., Steidel C. C., Fruchter A., 1996, *MNRAS*, 283, 1388
Mainini R., Macciò A. V., Bonometto S. A., Klypin A., 2003, *ApJ*, 599, 24
Marchesini D., van Dokkum P. G., Förster Schreiber N. M., Franx M., Labbé I., Wuyts S., 2009, *ApJ*, 701, 1765
Martin C. L., 2005, *ApJ*, 621, 227
McCarthy I. G., Schaye J., Font A. S., Theuns T., Frenk C. S., Crain R. A., Dalla Vecchia C., 2012, *MNRAS*, 427, 379
Moster B. P., Naab T., White S. D. M., 2013, *MNRAS*, 428, 3121
Moster B. P., Somerville R. S., Maulbetsch C., van den Bosch F. C., Macciò A. V., Naab T., Oser L., 2010, *ApJ*, 710, 903
Munshi F. et al., 2012, *ArXiv e-prints*
Murray N., Ménard B., Thompson T. A., 2011, *ApJ*, 735, 66
Murray N., Quataert E., Thompson T. A., 2010, *ApJ*, 709, 191
Noeske K. G. et al., 2007, *ApJL*, 660, L43
Oppenheimer B. D., Davé R., 2006, *MNRAS*, 373, 1265
Oppenheimer B. D., Davé R., 2008, *MNRAS*, 387, 577
Oppenheimer B. D., Davé R., Kereš D., Fardal M., Katz N., Kollmeier J. A., Weinberg D. H., 2010, *MNRAS*, 406, 2325
Pannella M. et al., 2009, *ApJL*, 698, L116
Peacock J. A., Smith R. E., 2000, *MNRAS*, 318, 1144
Pellegrini E. W., Baldwin J. A., Ferland G. J., 2011, *ApJ*, 738, 34
Peng Y.-j. et al., 2010, *ApJ*, 721, 193
Press W. H., Schechter P., 1974, *ApJ*, 187, 425
Puchwein E., Springel V., 2013, *MNRAS*, 428, 2966
Reed D., Governato F., Quinn T., Gardner J., Stadel J., Lake G., 2005, *MNRAS*, 359, 1537
Robotham A. S. G., Driver S. P., 2011, *MNRAS*, 413, 2570
Rujopakarn W. et al., 2010, *ApJ*, 718, 1171
Salim S. et al., 2007, *ApJS*, 173, 267
Santini P. et al., 2012, *A&A*, 538, A33
Sawala T., Guo Q., Scannapieco C., Jenkins A., White S., 2011, *MNRAS*, 413, 659
Schaye J., Dalla Vecchia C., 2008, *MNRAS*, 383, 1210
Sheth R. K., Mo H. J., Tormen G., 2001, *MNRAS*, 323, 1
Smolčić V. et al., 2009, *ApJ*, 690, 610
Somerville R. S., Primack J. R., 1999, *MNRAS*, 310, 1087
Springel V., Di Matteo T., Hernquist L., 2005, *MNRAS*, 361, 776
Springel V., Hernquist L., 2003, *MNRAS*, 339, 289
Stark D. P., Ellis R. S., Bunker A., Bundy K., Targett T., Benson A., Lacy M., 2009, *ApJ*, 697, 1493
Stark D. P., Schenker M. A., Ellis R., Robertson B., McLure R., Dunlop J., 2013, *ApJ*, 763, 129
Stinson G., Seth A., Katz N., Wadsley J., Governato F., Quinn T., 2006, *MNRAS*, 373, 1074
Stinson G. S., Brook C., Macciò A. V., Wadsley J., Quinn T. R., Couchman H. M. P., 2013, *MNRAS*, 428, 129
Thacker R. J., Couchman H. M. P., 2000, *ApJ*, 545, 728
van den Bosch F. C. et al., 2007, *MNRAS*, 376, 841
van der Burg R. F. J., Hildebrandt H., Erben T., 2010, *A&A*, 523, A74
Wadsley J. W., Stadel J., Quinn T., 2004, *New Astronomy*, 9, 137

- Weiner B. J. et al., 2009, *ApJ*, 692, 187
Weinmann S. M., Neistein E., Dekel A., 2011, *MNRAS*, 417, 2737
Weinmann S. M., Pasquali A., Oppenheimer B. D., Finlator K., Mendel J. T., Crain R. A., Macciò A. V., 2012, *MNRAS*, 426, 2797
Whitaker K. E. et al., 2011, *ApJ*, 735, 86
Whitaker K. E., van Dokkum P. G., Brammer G., Franx M., 2012, *ApJL*, 754, L29
White S. D. M., Frenk C. S., 1991, *ApJ*, 379, 52
White S. D. M., Rees M. J., 1978, *MNRAS*, 183, 341
Wilkins S. M., Trentham N., Hopkins A. M., 2008, *MNRAS*, 385, 687
Wuyts S. et al., 2011, *ApJ*, 738, 106
Yang X., Mo H. J., van den Bosch F. C., 2003, *MNRAS*, 339, 1057
Zheng X. Z., Dole H., Bell E. F., Le Flo'ch E., Rieke G. H., Rix H.-W., Schiminovich D., 2007, *ApJ*, 670, 301